Received: 1 November 2022 | Revised: 30 May 2023 | Accepted: 5 June 2023

DOI: 10.33012/navi.613

ORIGINAL ARTICLE

Satellite Constellation Design for a Lunar Navigation and Communication System

Sriramya Bhamidipati | **Tara Mina** | **Alana Sanchez** | **Grace Gao**

Department of Aeronautics and Astronautics, Stanford University

Correspondence
Grace Gao
Department of Aeronautics and Astronautics, Stanford University
Stanford, CA, USA, 94305
Email: gracegao@stanford.edu

Abstract

There has been a growing interest in using small satellites (SmallSats) for a future lunar navigation and communication satellite system (LNCSS). We conceptualize the design of a SmallSat-based LNCSS with Earth-global positioning system (GPS) time transfer that provides navigation and communication services near the lunar south pole. A hybrid constellation design is formulated, wherein all satellites provide navigation services while only a fraction are communication-enabled. Using Systems Tool Kit software, we examine various LNCSS case studies based on an elliptical lunar frozen orbit with a lower-grade chip-scale atomic clock. Case studies are evaluated in terms of (1) navigation considerations, including position and timing accuracy, lunar user equivalent ranging error, and dilution of precision, (2) communication considerations, including data volume, availability, and data rate, and (3) SmallSat factors, including cost, size, weight, and power. We performed a trade-off analysis for satisfying the criteria outlined by international space agencies while designing low-cost, low-SWaP lunar constellations.

Keywords

communication data rate, GPS, lunar satellite system, navigation accuracy, SmallSats, systems tool kit, time transfer

1 | INTRODUCTION

We are entering a second space race, with an emerging priority of the global exploration community to establish a sustainable human presence on the Moon. Moreover, more than 140 lunar missions are being planned for the next decade by international space agencies and commercial space companies, such as SpaceX, Rocket Lab, Argotec, and Blue Origin (Cohen et al., 2020; Tai et al., 2020). Among these missions, some notable ones include the National Aeronautics and Space Administration (NASA) Artemis mission, the China National Space Administration's Chinese lunar exploration program, and the European Space Agency (ESA) European large logistics lander project. To support upcoming plans for both human and robotic activities on the lunar surface, reliable, real-time navigation and communication services are crucial.

Active efforts are being invested in designing a dedicated satellite constellation for the Moon. As outlined in NASA's Space Communication Architecture Working

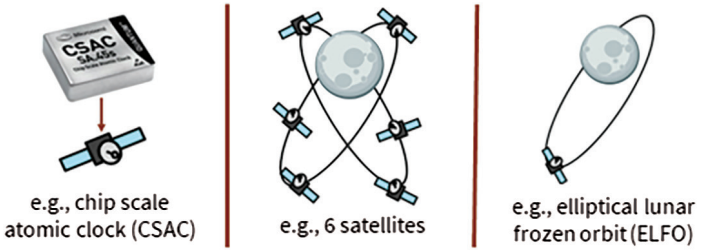

FIGURE 1 Example design choices, namely, the satellite clock, constellation size, and orbit, to be finalized during the design of a SmallSat-based LNCSS

Group (SCAWG) report (National Aeronautics and Space Administration, 2006) and NASA's preliminary lunar relay services requirements document (SRD) (National Aeronautics and Space Administration, 2022), these lunar satellites will provide navigation and communication signals for missions in the south pole region in the near future and for the broader lunar surface (global coverage) in the long term. The Moon's south pole region (comprising southern latitudes greater than 80° (National Aeronautics and Space Administration, 2022)) is a key region of interest (Flahaut et al., 2020), given the recent discovery of water ice deposits in its permanently shadowed craters, such as Shackleton, Shoemaker, Faustini, and Haworth. To provide satellite-based navigation and communication services, NASA has conceptualized the LunaNet framework (Israel et al., 2020), and the ESA has begun work on its Moonlight initiative (Cozzens, 2021). Additionally, an Italian space company called Argotec and NASA's Jet Propulsion Laboratory are collaborating on a lunar constellation concept called ANDROMEDA. NASA has also expressed interest in using a small satellite (SmallSat) platform for the future lunar constellation, as SmallSats are cost-effective, easily scalable, and rapidly deployable (Israel et al., 2020). We refer to the dedicated lunar constellation providing navigation and communication services as a lunar navigation and communication satellite system (LNCSS).

Our work focuses on designing a SmallSat-based LNCSS that serves the lunar south pole region while considering the following design criteria: i) adequate accuracy of user position and receiver clock timing and ii) sufficient daily volume of communication data transfer to/from Earth. Note that the long-term goals of the LNCSS include global availability of these services and communication connectivity among lunar assets, which will be addressed in future work. Given that lunar constellation initiatives are in their preliminary stages, many key design considerations are yet to be finalized. Some examples of design considerations, as shown in Figure 1, include the satellite clock, constellation size, lunar orbit, and so on. For example, because the Moon has an anisotropic gravitational field, a potential lunar orbit investigated in recent literature (Ely & Lieb, 2006) is the elliptical lunar frozen orbit (ELFO). This interest has arisen because ELFOs minimize sensitivity to external perturbations for providing persistent, stable coverage to either the north or south pole with no requirement for station-keeping, i.e., $\Delta V_{10\,yrs} \approx 0$.

1.1 | LNCSS Constellation Design Criteria and Performance Metrics

The navigation service performance of a SmallSat-based LNCSS design can be analyzed using various metrics, including the following (National Aeronautics and Space Administration, 2006, 2022):

- Lunar user equivalent ranging error (UERE): Quantifies the ranging accuracy of transmitted satellite signals
- Geometric dilution of precision (GDOP): Evaluates the geometry of LNCSS satellites with respect to the lunar user, which in turn affects the expected position and timing error covariances
- Navigation service availability: Denotes the percentage of time during which a navigation solution can be estimated for a lunar user at a given point on the Moon (equivalent to the percent visibility of at least four LNCSS satellites)
- Navigation service coverage: Denotes the percentage of area of the lunar south pole at which navigation services are available
- Navigation service failure tolerance: Denotes the navigation service availability for a lunar user at a given point on the Moon, under a single-satellite failure (equivalent to the percent visibility of at least five LNCSS satellites)

Similarly, one can evaluate the communication service performance of an LNCSS design in terms of various metrics, including the following (National Aeronautics and Space Administration, 2006, 2022):

- Data rate: Denotes the rate of communication data transfer between the lunar user and Earth
- Communication service availability: Denotes the percentage of time for which a communication link between a lunar user and Earth can be maintained (equivalent to the percent visibility of at least one LNCSS satellite)
- Communication service coverage: Determines the percent area of the lunar south pole at which communication services are available
- Communication service failure tolerance: Denotes the communication service availability for a lunar user (at a given point on the Moon), under failure of any one satellite (equivalent to the percent visibility of at least two LNCSS satellites)

Additionally, other SmallSat factors influencing the LNCSS design are as follows:

- Delta-V for station-keeping: Denotes a measure of orbital stability, i.e., maneuvers required to maintain the desired orbit in the presence of higher perturbations due to the weak lunar gravity field and the strong third-body perturbations from Earth
- Size, weight, and power (SWaP) of the onboard equipment: Accounts for the limited payload capacity of the SmallSat platform
- Overall cost: Accounts for one-time costs and recurring costs
  Note that one-time costs include the development cost of a satellite and its onboard equipment, launch costs from Earth, and injection costs for inserting a satellite into a lunar orbit from a transfer orbit. Recurring costs include the production costs of an entire constellation, replacement costs of end-of-mission-life satellites, maintenance costs related to health checks, and operation costs such as costs related to the Deep Space Network (DSN)-based tracking network (if relevant), uplink of corrections to onboard timing, and ephemeris (if relevant).

Note that this work's focus is on assessing which design considerations influence satellite-level and constellation-level choices, whereas accounting for other factors, such as hardware design, link budget, signal strength, and lunar user burden, will be explored in future works.

1.2 | Preliminary Design and Performance Requirements

Although NASA has outlined key design criteria and performance considerations for a future LNCSS, no well-defined quantitative standards currently exist. However, some preliminary needs have been identified by international space agencies and commercial space companies based on future lunar mission needs. For instance, the global exploration community targets a three-dimensional (3D) positioning accuracy below 50 m to be provided by the lunar satellite constellation (Cozzens, 2021). Moreover, the NASA SRD (National Aeronautics and Space Administration, 2022) quantifies the desired knowledge of 3σ horizontal position for lunar surface users to be less than 10 m and 3σ timing to be within 0.1 ms. Additionally, the real-time knowledge onboard any LNCSS satellite is expected to be within a 1σ position of 4 m, 1σ velocity of 0.4 m/s, and 1σ timing of 20 ns (National Aeronautics and Space Administration, 2022). Furthermore, in terms of communication service reliability, the daily data volume between a lunar user and Earth is prescribed to satisfy $\geq$ 160 GB (Rimani et al., 2021), 240–2400 GB (European Space Agency, 2021), or at least 600 GB (Schier, 2022). For reference, the daily volume of data transmitted by the Lunar Reconnaissance Orbiter (LRO), which was launched in 2009, is 461 GB (National Aeronautics and Space Administration, 2009). In addition, the high data rate services for the return link (i.e., lunar user to Earth) are expected to be 5–100 Mbps (National Aeronautics and Space Administration, 2022).

1.3 | Related Work

There exist rich preliminary studies on the design of future lunar constellations. However, these prior works do not explore all of the navigation and communication design criteria and performance metrics from a SmallSat perspective, as outlined in Section 1.1.

With regards to the lunar constellation design, the authors of Murata et al. (2022) designed an ELFO-based constellation, wherein they assess the navigation performance at the lunar south pole using the dilution of precision (DOP), satellite visibility, and position accuracy. To provide global lunar coverage, prior works (Pereira & Selva, 2020, 2022) have investigated design trade-offs among various constellations with near-circular polar orbits and frozen orbits by evaluating their DOP, position accuracy, delta-V, and overall cost. In Nallapu et al. (2020), the authors designed a halo-orbit-based lunar constellation to address only communication-related requirements, namely, coverage, synchronization, and received power. Another orbital study (Iannone et al., 2021) investigated the navigation service performance of Walker orbits and ELFOs in terms of availability, DOP, and SmallSat factors, namely, station-keeping needs and overall cost. In Thompson et al. (2010), the authors discussed preliminary criteria related to navigation and communication for lunar constellations based on frozen and halo orbits. Prior work (Hamera et al., 2008) presented a low-cost lunar constellation concept using SmallSats in halo orbits, wherein the designs are evaluated based on position accuracy, overall cost, orbital stability, communication availability, and communication coverage.

To meet the stringent SWaP requirements onboard a SmallSat-based LNCSS, one strategy is to opt for a lower-grade satellite clock instead of a higher-grade clock. The grade of the satellite clock, which determines the timing stability and affects the navigation ranging precision and communication time synchronization offered to lunar users, is critical for designing a reliable navigation and communication

system. Although using a lower-grade clock for an LNCSS limits its timing stability, one can intelligently mitigate this shortcoming by harnessing the signals already being broadcast by the legacy Earth-GPS constellation. Utilizing Earth-GPS signals for various lunar applications has been an active research topic in recent times, especially since the occurrence of the following major events: a) NASA's antenna characterization experiment (Donaldson et al., 2020) modeled the signal performance in Earth-GPS transmit antenna side lobes and b) recent simulation studies (Capuano et al., 2015; Winternitz et al., 2019) designed a high-sensitivity Earth-GPS receiver and confirmed the successful acquisition of Earth-GPS signals at lunar distances, despite significantly attenuated levels of signal power. Given these early successes, there is great potential in integrating a lower-grade clock with an Earth-GPS receiver to maintain desired timing accuracy onboard a SmallSat-based LNCSS satellite.

In prior works (Bhamidipati et al., 2021, 2022a), we proposed the design of a SmallSat-based lunar navigation satellite that utilizes available Earth-GPS signals (when not occluded by Earth or the Moon) to estimate the timing corrections of a lower-grade satellite clock. A formulation of a lunar UERE was devised that primarily depends on the root-mean-square (RMS) timing error in the time transfer from the Earth GPS. In another prior work (Bhamidipati, Mina, & Gao, 2022b), a case study analysis was performed, wherein the trade-off between different grades of satellite clocks and lunar orbits in designing a lunar navigation satellite with Earth-GPS time transfer was analyzed. We demonstrated a lunar UERE that was comparable to that of the Earth GPS across various case studies, even with low-SWaP clocks, such as a chip-scale atomic clock (CSAC) (Schmittberger & Scherer, 2020).

1.4 | Proposed Idea and Key Contributions

In Figure 2, the design of a SmallSat-based LNCSS with Earth-GPS time transfer that provides both navigation and communication services at the lunar south pole is conceptualized. A hybrid constellation design is developed, wherein all satellites provide navigation services but only a fraction are additionally enabled with communication services. By selectively equipping only some satellites in the LNCSS constellation with a communication payload, space segment costs are saved and the onboard SWaP is reduced (Sections 3.3.3) and 3.2.5) demonstrate that the LNCSS satellite's average cost and onboard SWaP are congruent with NASA's low-budget SmallSat missions).

In this work, various LNCSS constellation case studies are formulated and evaluated based on design criteria and performance metrics of navigation and communication, as well as SmallSat factors. As explained earlier, the navigation service reliability is assessed in terms of position and timing accuracy, which represent the design criteria, while the lunar UERE, GDOP, availability, coverage, and failure tolerance are considered as navigation performance metrics. Similarly, the communication service reliability is assessed in terms of sufficient daily volume of data transfer to/from Earth, which represents the key design criteron, while the data rate, availability, coverage, and failure tolerance are considered as additional performance metrics of the communication service. SmallSat factors are also heuristically evaluated, including the onboard SWaP and space segment cost, which is an important component of the overall cost outlined above.

To account for SmallSat constraints on the LNCSS constellation design, time transfer is performed using an onboard Earth-GPS receiver (i.e., whenever at least

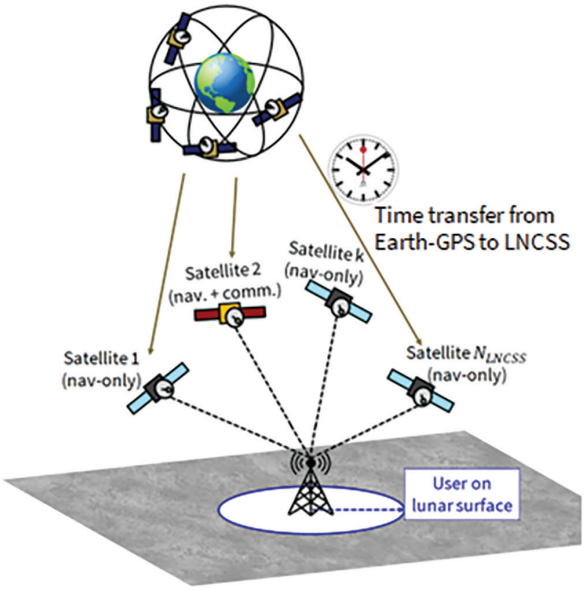

FIGURE 2 Architecture of this work's SmallSat-based LNCSS with Earth-GPS time transfer that provides both navigation and communication services at the lunar south pole region
In this hybrid constellation design, only a few satellites among the LNCSS constellation are enabled to provide communication services, while all of the LNCSS satellites provide navigation services.

one Earth-GPS satellite is visible) to compute timing corrections for a low-cost onboard clock. To execute this time transfer, unlike prior works (Bhamidipati et al., 2021, 2022a, 2022b), a three-state Kalman filter is formulated that accounts for nonlinearities in clock state propagation by estimating the clock drift rate in addition to the clock bias and drift states. A modified lunar UERE (navigation performance metric) is estimated by first computing a broadcast clock component, which depends on the filter estimation error from Earth-GPS time transfer. The attainable data rate (communication performance metric) is also modeled between an LNCSS satellite and Earth, which, among other factors, depends on the received signal-to-noise ratio (SNR). The SNR is influenced by the bit error rate, which in turn depends on the filter estimation error. Indeed, the proposed Earth-GPS time transfer affects both the navigation lunar UERE and communication data rate and thereby influences both navigation and communication design criteria from a SmallSat perspective.

This study is based on prior work (Bhamidipati, Mina, Sanchez, et al., 2022), and the key contributions of this work are as follows:

1. We conceptualize an LNCSS with time transfer from the Earth GPS, wherein all satellites are enabled to provide navigation services at the lunar south pole with a fraction of the satellites additionally providing communication services.
2. We design a three-state Kalman filter that harnesses legacy Earth-GPS signals to estimate the bias, drift, and drift rate of a low-cost onboard clock. Based on these estimates, a modified lunar UERE metric (as compared with our prior work (Bhamidipati et al., 2021, 2022b)) is devised, and the data rate that can be attained for communication between an LNCSS satellite and Earth is determined.
3. We develop three LNCSS case studies involving ELFO-based constellation designs. In particular, case studies are formulated by varying the orbital parameters, number of orbit planes, and satellites per plane. Additionally,

different elevations that a user at the lunar south pole might encounter are investigated, i.e., a low mask angle in open-sky settings and a high mask angle in restricted satellite visibility regions, such as in a lunar crater.

4. We assess the trade-offs across different LNCSS case studies based on whether the design criteria and performance metrics for navigation and communication services as well as SmallSat factors comply with the preliminary requirements proposed by various stakeholders such as NASA, the ESA, and commercial space agencies. As discussed earlier, navigation-related design criteria are assessed in terms of positioning and timing accuracy achieved whereas communication-related criteria are evaluated based on the daily volume of data transferred to/from Earth.

2 | SMALLSAT-BASED LNCSS WITH EARTH-GPS TIME TRANSFER: DESIGN AND PERFORMANCE CONSIDERATIONS

We describe the mathematical formulation of an Earth-GPS time transfer that performs clock estimation. Note that, we consider the clock estimation technique to be decoupled from that of orbit estimation in the Earth-GPS time-transfer design, i.e., position and velocity of the LNCSS satellite is obtained from known/pre-computed ephemeris. For more details, please refer to our prior work (Bhamidipati, Mina, & Gao, 2022a), wherein clock estimation errors are analyzed as broadcast ephemeris errors onboard an LNCSS satellite are varied across different orders of magnitude. Addressing the correlation between the onboard clock and the orbital trajectory of an LNCSS satellite is an important task, which will be explored in future works. Navigation and communication design considerations are also explained from the perspective of a SmallSat platform and hybrid lunar constellation.

2.1 | Modified Earth-GPS Time-Transfer Design

Compared with prior works (Bhamidipati et al., 2021, 2022a, 2022b) that utilized a linear two-state clock model, a three-state Kalman filter is designed in this work. This modified filter accounts for the nonlinearities of a lower-grade onboard clock while harnessing the Earth-GPS signals (when available). For any LNCSS satellite, the filter maintains the LNCSS clock estimate at each time epoch t by propagating the following state vector: $x_t := [b_t, \dot{b}_t, \ddot{b}_t]^\top$, where b_t is the clock bias state in m, $\dot{b}_t$ is the clock drift in ms^{-1}, and $\ddot{b}_t$ is the clock drift rate in ms^{-2}, with units converted from the timing domain through multiplication by the speed of light, $c = 299792458$ m/s. The equations derived in Zucca and Tavella (2005) are closely followed to model the time and measurement update equations.

In the timing filter, a time update is performed every Δt seconds to estimate the predicted state vector based on the clock error propagation model shown in Equation (1). In addition, the state covariance matrix is propagated according to Equation (2), where the process noise covariance Q is defined in terms of diffusion coefficients $\sigma_1, \sigma_2, \textit{and } \sigma_3$: These diffusion coefficients represent the intensity of noise in each state (Zucca & Tavella, 2005):

$$\bar{x}_t = Ax_{t-1} + \mu_3 G \tag{1}$$

$$\bar{P}_t = AP_{t-1}A^\top + Q \tag{2}$$

where $\bar{x}_t$ and $\bar{P}_{t-1}$ are the predicted state vector and state error covariance matrix at time step t, respectively, x_{t-1} and P_{t-1} are the corrected state vector and state error covariance matrix at time step $t-1$, respectively, and μ_3 denotes the linear coefficient of the time variation of the clock drift rate. The process noise covariance matrix Q is defined as follows:

$$Q = \begin{bmatrix} \sigma_1^2\Delta t + \sigma_2^2\Delta t^3/3 + \sigma_3^2\Delta t^5/20 & \sigma_2^2\Delta t^2/2 + \sigma_3^2\Delta t^4/8 & \sigma_3^2\Delta t^3/6 \\ \sigma_2^2\Delta t^2/2 + \sigma_3^2\Delta t^4/8 & \sigma_2^2\Delta t + \sigma_3^2\Delta t^3/3 & \sigma_3^2\Delta t^2/2 \\ \sigma_3^2\Delta t^3/6 & \sigma_3^2\Delta t^2/2 & \sigma_3^2\Delta t \end{bmatrix} \tag{3}$$

The state transition matrix A is defined by $A = \begin{bmatrix} 1 & \Delta t & \Delta t^2/2 \\ 0 & 1 & \Delta t \\ 0 & 0 & 1 \end{bmatrix}$, and the control matrix G is defined by $G = \begin{bmatrix} \Delta t^3/3 \\ \Delta t^2/2 \\ \Delta t \end{bmatrix}$.

The diffusion coefficients $\sigma_1, \sigma_2,$ *and* σ_3 can be written in terms of h_0 and h_{-2}, which are the power spectral density coefficients obtained from an Allan deviation plot (Krawinkel & Schön, 2015). Comparing Equations (6) and (8) from Van Dierendonck and McGraw (1984) with Equations (46) and (48) from Zucca and Tavella (2005), $\sigma_1 = \sqrt{\frac{h_0}{2}}$ and $\sigma_2 = \sqrt{2\pi^2 h_{-2}}$. Additionally, in this work, the frequency drift is considered to be constant, which implies that $\sigma_3 = 0$ (Zucca & Tavella, 2005).

To execute the measurement update step, i.e., to perform a time transfer from the Earth-GPS, the received carrier-to-noise density ratio (C/N_0) is first assessed to evaluate whether at least one Earth-GPS satellite is visible, as also done in prior work (Bhamidipati et al., 2021, 2022b). Then, the expected pseudorange and pseudorange rates are determined from the visible Earth-GPS satellites to form a measurement vector of residuals. The measurement vector $z_t \in \mathbb{R}^{2N_{eGPS,t}\times 1}$ is as follows:

$$z_t := \begin{bmatrix} \tilde{\rho}_t^{(1)} & \cdots & \tilde{\rho}_t^{(N_{eGPS,t})} & \dot{\tilde{\rho}}_t^{(1)} & \cdots & \dot{\tilde{\rho}}_t^{(N_{eGPS,t})} \end{bmatrix}^\top \tag{4}$$

where $N_{eGPS,t}$ is the total number of visible Earth-GPS satellites at time t and $\tilde{\rho}_t^{(k)}$ and $\dot{\tilde{\rho}}_t^{(k)}$ are the pseudorange and pseudorange rate residuals, respectively, from satellite k. The pseudoranges and pseudorange rates provide information about clock bias and clock drift, respectively.

With the measurement vector and modeled measurement covariance, the filter applies corrections to the predicted timing state via standard Kalman filter expressions to obtain the updated state vector x_t and state covariance P_t. In this work, the measurement model C_t is defined in accordance with the three-state vector $C_t \in \mathbb{R}^{2N_{eGPS,t}\times 3}$ as follows:

$$C_t = \begin{bmatrix} 1_{N_{eGPS,t}\times 1} & 0_{N_{eGPS,t}\times 1} & 0_{N_{eGPS,t}\times 1} \\ 0_{N_{eGPS,t}\times 1} & 1_{N_{eGPS,t}\times 1} & 0_{N_{eGPS,t}\times 1} \end{bmatrix}, \quad (\text{where } z_t = C_t x_t) \tag{5}$$

where $0_{a\times b}$ represents a matrix with size $a\times b$ of zeros and $1_{a\times b}$ represents a matrix with size $a\times b$ of ones. Additionally, the measurement covariance matrix is

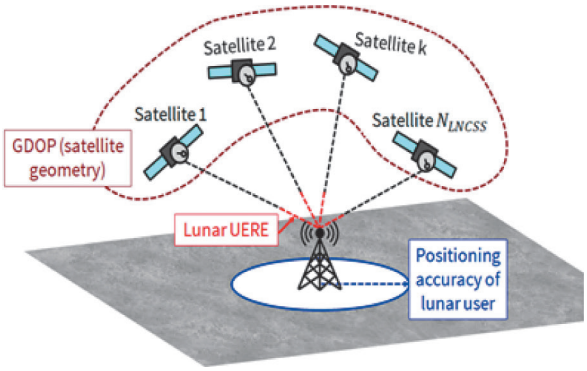

FIGURE 3 Illustration of the navigation design criteria and their dependency on two performance metrics, namely, lunar UERE and GDOP

modeled as a time-dependent diagonal matrix, based on the tracking errors of the receiver delay lock loop, phase lock loop, and Earth-GPS UERE (different from that of the lunar UERE). This work discards the Earth-GPS signals that pass through Earth's atmosphere. An investigation of other options, such as modeling Earth's atmosphere effects or formulating ionospheric-free Earth-GPS measurements, is left as an extension for future work.

2.2 | Navigation Service Design Considerations

As shown in Figure 3, the navigation design criteria, which involve achieving adequate position and timing accuracy, mathematically depend on the product of two performance metrics, namely, the lunar UERE and GDOP. The other three performance metrics discussed in Section 1, namely, availability, coverage, and failure tolerance, influence when, where, and for how long the navigation services are available. These three performance metrics are largely governed by the number of visible LNCSS satellites at the lunar south pole region.

Prior works (Bhamidipati et al., 2021, 2022b) have provided an in-depth breakdown of the lunar UERE formulation, utilizing the fact that, unlike Earth, the Moon does not have an atmosphere and buildings. Therefore, the error sources included in the lunar UERE metric, denoted by $\sigma_{\text{UERE, LCNSS}}$ in Equation (6), are the broadcast clock $\sigma_{\text{clk, LNCSS}}$, group delay $\sigma_{\text{gd, LNCSS}}$, broadcast ephemeris $\sigma_{\text{eph, LCNSS}}$, and receiver noise $\sigma_{\text{rec, LNCSS}}$. The broadcast clock component depends on the error in estimating timing corrections from the Earth-GPS time transfer. Note that the error sources caused by the LNCSS satellite attitude errors and the antenna phase center offsets are considered to be minor in comparison and thus negligible:

$$\sigma_{\text{UERE,LCNSS}} = \sqrt{\sigma^2_{\text{clk,LNCSS}} + \sigma^2_{\text{gd,LNCSS}} + \sigma^2_{\text{eph,LCNSS}} + \sigma^2_{\text{rec,LNCSS}}} \tag{6}$$

2.3 | Communication Service Design Considerations

The communication design criteria, which involve ensuring sufficient daily data volume to and from Earth, depend on the attainable data rate. Figure 4 illustrates how the communication between lunar users and Earth consists of two key communication links (National Aeronautics and Space Administration, 2022): one

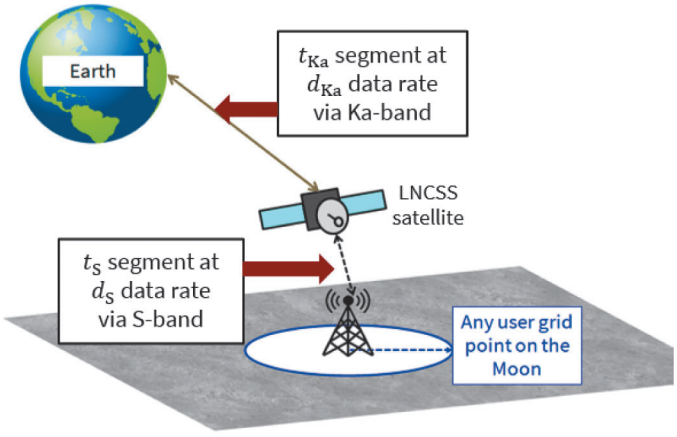

FIGURE 4 Data communication between the lunar surface and Earth consists of two data links: One between the LNCSS and Earth (via the Ka-band) and one between the LNCSS and the lunar user (via the S-band)
Both data links together influence the total amount of daily data transfer possible between the lunar surface and Earth, also called the *daily data volume*.

between the LNCSS and Earth via the Ka-band and one between the LNCSS and the lunar user via the S-band. Note that the frequency bands for lunar communications are pre-allocated (National Aeronautics and Space Administration, 2022), wherein the Ka-band is assigned for long-range and the S-band is allocated for lunar-satellite-to-surface-user communications. Both data links have an associated data rate, denoted as d_{Ka} for the LNCSS–Earth data link in the Ka-band and d_S for the LNCSS–user link in the S-band. The two data links also both have an associated summed daily availability for data transfer across all communication satellites, similarly denoted as t_{Ka} and t_S in Figure 4.

Apart from the data rate, the other communication performance metrics discussed in Section 1, namely, the availability, coverage, and failure tolerance, influence when, where, and for how long the services are available. These three performance metrics depend on the number of communication-enabled LNCSS satellites visible at the lunar south pole region.

Mathematically, the daily data volume through each communication link, or the amount of data that can be transferred per day through each link, is as follows:

$$D_{Ka} = d_{Ka} t_{Ka} \tag{7}$$

$$D_S = d_S t_S \tag{8}$$

where the 'Ka' subscript denotes terms for the Ka-band and the 'S' subscript denotes terms for the S-band, d_{Ka} and d_S are denoted in bits/second (bps), and t_{Ka} and t_S are denoted in seconds. For instance, given an LNCSS constellation with one communication-enabled satellite, $t_{Ka} < 86400$ s, whereas with two communication-enabled satellites, $t_{Ka} < 172800$ s. Because any data transfer must occur through both communication links, the total daily data volume D for communications between the lunar user and Earth is evaluated as follows:

$$D = \min\left(D_{Ka}, D_S\right) \tag{9}$$

Given that the lunar surface can have multiple users sending data simultaneously to any visible LNCSS satellite, D_S is generally expected to depend on the number of users and could be larger than D_{Ka} once multiple users are deployed

on the lunar surface. Furthermore, for any scientific data collected from the lunar surface, to ensure maximal scientific return and to reduce the data storage burden for LNCSS satellites, D_{Ka} is required to be comparable to or greater than D_{S}.

This work focuses on analyzing the LNCSS–Earth daily data volume D_{Ka}, given that this component of the communication link could become a potential bottleneck in the total data transfer and scientific return from lunar missions. The uplink/downlink between LNCSS and Earth is considered available when there is a direct line of sight between at least one communication-enabled LNCSS satellite and the center of Earth. To keep this analysis more generalized, the definition of the Earth support system is assumed to be abstract, with statistics calculated with respect to the center of Earth rather than a specific set of ground stations such as DSN.

To compute the attainable data rate between an LNCSS satellite and Earth, an approach similar to the one outlined by Nallapu et al. (2020) is followed. First, the minimum SNR needed to achieve a desired bit error rate for communications must be evaluated (Proakis & Salehi, 2008), which is related via the following expression for a communication system with binary phase shift keying modulation:

$$\frac{E_b}{N_0} = (\text{erfc}^{-1}(2B_{\text{ER}}))^2 \tag{10}$$

where $\frac{E_b}{N_0}$ is the minimum SNR required to satisfy the desired bit error rate B_{ER} and erfc^{-1} is the inverse complementary error function, which is closely related to the complementary cumulative distribution function of a standard normal Gaussian random variable (Proakis & Salehi, 2008). From this minimum required SNR, the minimum data rate of reception (Nallapu et al., 2020) can be computed as follows:

$$d_{min} = \frac{P_{\text{rx,min}}}{kT_{\text{rx}}\left(\frac{E_b}{N_0}\right)}\sin^2\beta \tag{11}$$

where $k = 1.380649 \cdot 10^{-23}$ m^2 kg s^{-2} K^{-1} is the Boltzmann constant, T_{rx} is the noise temperature level in Kelvin, β is the phase modulation index, $\frac{E_b}{N_0}$ is the required SNR computed from Equation (10), and $P_{\text{rx,min}}$ is the minimum received power level in watts. The minimum received power level is also computed following an approach similar to that of Nallapu et al. (2020), i.e., as a function of the transmitted power P_{tx}, the receiver and transmitter gain factors G_{rx} and G_{tx}, the frequency of transmission f_{tx}, and the maximum distance between the ground station and the LNCSS satellite r_{max}, according to Friis' transmission formula (Stutzman & Thiele, 2013):

$$P_{rx,\text{min}} = \frac{P_{\text{tx}}G_{\text{rx}}G_{\text{tx}}}{\left(4\pi r_{\text{max}}\frac{f_{\text{tx}}}{c}\right)^2} \tag{12}$$

where the transmitter gain G_{tx} is determined from the antenna properties, including the antenna efficiency and antenna diameter (Nallapu et al., 2020).

2.4 | SmallSat Factors

Among the SmallSat factors discussed in Section 1, delta-V is specific to the lunar orbit chosen, whose formulation based on orbital dynamics is beyond the scope of

this paper. Cost analysis for this work focuses on the empirical formulation of cost and SWaP related only to the space segment, which serves as one of the key components in LNCSS constellation design. Note that evaluations of other components of the overall cost related to launch, maintenance, and injection will be explored in future works.

For any LNCSS constellation design, the total space segment cost is formulated as a sum of the total development cost and total production cost. The total development cost denotes the non-recurring cost component incurred in designing one satellite unit (or a specific unit of onboard equipment). Meanwhile, the total production cost denotes the recurring cost component incurred in producing any desired number of satellite units (or desired units of onboard equipment). These costs are computed for the hybrid constellation design, for which the LNCSS constellation size is defined as N_{LNCSS} and the number of navigation- and communication-enabled satellites among them as N_{comm} with $N_{comm} < N_{LNCSS}$. The development cost is broken down into a summation of development costs associated with a communication payload and the costs for a navigation-only satellite. Similarly, the production cost is also broken down into the cost of producing N_{LNCSS} navigation-only satellites and the cost of producing N_{comm} communication payloads. Note that the development cost primarily depends on mass, while the production cost depends on the first unit cost and the number of units to be produced (Hirshorn et al., 2017; Wertz et al., 2011).

To evaluate the space segment cost, each of the following four cost components are computed individually: the development cost of a communication payload, the production cost of N_{comm} communication payloads, the development cost of a navigation-only satellite, and the production cost of N_{LNCSS} navigation-only satellites.

Firstly, the development cost of a communication payload $Y_{dev-comm}$ is computed based on a derivation by Esper (2022). This cost, in fiscal year (FY) 2010 million dollars, is as follows:

$$Y_{dev-comm} = \left(339 m_{comm} + 5127 L\right)/1000.0 \tag{13}$$

where L denotes the number of communication channels and m_{comm} is defined as the communication payload mass, which is computed by leveraging the Magellan high-gain antenna design for an empirical dish diameter (Brown, 2002). In particular, $m_{comm} = N_{channels} N_{ant} \left(2.89 D_{ant}^2 + 6.11 D_{ant} - 2.59\right)$, with $N_{channels}$ as the number of communication channels onboard a satellite, N_{ant} as the number of onboard communication antennae required for each channel, and D_{ant} as the antenna diameter. Note that $N_{ant} \geq 2$ because an LNCSS communication satellite requires at least two communication antennae: one to communicate with lunar users and one to transmit data to/from Earth.

Next, the development cost of a navigation-only satellite $Y_{dev-nav}$ is computed based on a derivation by Wertz et al. (2011). This cost, in FY2010 million dollars, is as follows:

$$Y_{dev-nav} = 110.2 m_{nav}/1000.0 \tag{14}$$

where m_{nav} is defined as the total mass of a navigation-only satellite, which is also computed heuristically.

To compute the total mass m_{nav} of a navigation-only satellite, the payload equipment onboard a navigation-only LNCSS satellite is broken down and the total payload power $P_{payload-nav}$ is computed. Next, the data from past deep space missions

are mapped to estimate the corresponding total payload mass m_{nav} (Wertz et al., 2011). Based on Bhamidipati et al. (2021, 2022b), European Space Agency (2023), Pereira and Selva (2020), the payload equipment onboard the navigation-only LNCSS satellite includes the following: lower-grade satellite clock, Earth-GPS receiver, navigation signal generation unit, frequency generation and upconversion unit, and remote terminal unit. The total payload power $P_{payload-nav}$ is computed as the sum of the power required by individual payloads. Then, from the total payload power, the payload mass is finally estimated in kilograms as $m_{nav} = 38(0.14P_{payload-nav})^{0.51}$ (Wertz et al., 2011). The specific power levels for each component are detailed in Section 3.2.5).

The same heuristic relationship shown in Equation (15) is followed to compute the total production costs for communication payloads and for navigation-only satellites:

$$Y_{prod-comm} \text{ or } Y_{prod-nav} = T_1 N\left(1 + \frac{ln(S)}{ln2}\right) \tag{15}$$

where T_1 depicts the first unit cost and S represents a predefined learning rate.

For instance, to compute the total production cost for communication payloads $Y_{prod-comm}, T_1$ is heuristically computed as $T_1 = 189m_{comm}/1000$ and $N = N_{comm}$ is assigned. In contrast, to compute the total production cost for navigation-only satellites $Y_{prod-nav}, T_1$ is heuristically computed from past mission data as $T_1 = \left(289.5m_{comm}^{0.719}\right)/1000$ (Pereira & Selva, 2020; Wertz et al., 2011) and $N = N_{LNCSS}$ is assigned.

Note that all of the above formulae hold true for FY2010; therefore, each computed cost component must be scaled by an appropriate inflation factor to compute the total space segment cost. The inflation factors for conversions from 2010 up until 2036 are the same as those suggested by Table 11–9 of Wertz et al. (2011).

3 | LNCSS CASE STUDIES AND COMPARISON ANALYSIS

Various LNCSS case studies are evaluated using simulated experimental data, and then, trade-offs are analyzed among these studies in terms of design criteria and performance metrics for navigation and communication services, as well as SmallSat factors.

3.1 | Overview of LNCSS Case Studies

For this case study analysis, three LNCSS designs are examined, wherein each satellite is equipped with a navigation unit, an onboard CSAC, an Earth-GPS receiver, and a communication unit (if applicable).

3.1.1 | ELFO-Based Flower Constellation Setup

The LNCSS case studies are based on an ELFO. As mentioned in Section 1, an ELFO refers to a specific category of *frozen orbits* with a highly elliptical shape for providing greater coverage of the lunar poles. Here, *frozen* orbits are orbits that maintain nearly constant orbital parameters for extensive periods of time, without requiring station-keeping (Folta & Quinn, 2006; Whitley & Martinez, 2016).

Furthermore, the case studies are based on flower constellations (McManus & Schaub, 2016; Mortari et al., 2004), in which each orbital plane depicts a flower petal. Unlike constellation patterns such as Walker-Delta or Walker-Star patterns, the flower constellations belong to a special family of J2-frozen repeat ground track constellations wherein the orbital parameters are selected such that the nodal period of the orbit matches the nodal period of the primary body (in this case, the Moon) by a factor that depends on the number of days and the number of revolutions needed to repeat the ground track. Within a flower constellation, all satellites have identical orbital elements, except for the right ascension of the ascending node (RAAN) and the initial mean anomaly, which are chosen based on the desired phasing scheme.

To derive the orbital parameters for the LNCSS constellation case studies, the frozen orbit equations used by Ely and Lieb (2006) are closely followed, which are expressed in the Earth orbital plane (OP) frame. Ely (2005) and Ely and Lieb (2006) define the x-axis of the OP frame by the intersection of the Moon's equatorial plane with Earth's apparent orbital plane, the z-axis by the direction of the orbit normal to Earth's apparent orbit around the Moon, and the y-axis as completing the triad. Note that the OP frame is not an inertial frame, as its unit vectors exhibit slow variations over time with respect to the Moon's J2000 frame, which is an inertial frame.

All LNCSS case studies and all satellites within each case study are considered to have the same eccentricity, inclination, semi-major axis, and argument of perigee (see Table 1). In particular, the eccentricity variations for the ELFO range between 0.6 and 0.7 (Ely, 2005), based on which an eccentricity of $e = 0.6$ is assigned. Furthermore, the inclination $i = 51.7°$ is computed using the relationship $e^2 + (5/3)\cos^2 i = 1$, which is obtained by solving the simplified equations for the mean motion of the satellite orbits (Ely & Lieb, 2006). By analyzing these simplified equations, Ely and Lieb (2006) computed the argument of perigee solutions to be $\omega = 90°$ or 270°; thus, the argument of perigee was set to $\omega = 90°$ to maximize the service coverage over the lunar south pole region. With the radius of the Moon as $R_M = 1734$ km, the semi-major axis is incorporated by considering the perigee altitude $h_{perigee} = 720$ km and apogee altitude $h_{apogee} = 8090$ km (Balossino & Davarian, 2022). The apogee altitude ensures service reliability with S-band communication at the south pole, even when the distance between the communication antenna of the onboard LNCSS satellite and the lunar user is at its farthest. Again, borrowing the inequalities used by Ely and Lieb (2006) that determine the relationship between eccentricity and semi-major axis, i.e., $a(1-e) - R_M \geq h_{perigee}$ and $a(1+e) - R_M \leq h_{apogee}$, the semi-major axis was set to a = 6143 km. Based on

TABLE 1
Orbital Parameters Represented in the OP Frame for the Three LNCSS Constellation Case Studies
The short-hand notation $x : y : z$ indicates a series generated within the closed interval $[x, z]$, with spacing between values given by y. Note that for any case study, all combinations of the RAAN and mean anomaly series are considered to generate the orbital parameters: e.g., the 8 satellites in case study A are given by the following [RAAN, mean anomaly] pairs: [0, 0], [0, 90], [0, 180], [0, 270], [180, 0], [180, 90], [180, 180], [180, 270].

LNCSS Case Study	No. of Satellites	Semi-Major Axis a (km)	Eccentricity e	Inclination i (deg)	Argument of Perigee ω (deg)	RAAN Ω	Mean Anomaly M
A	8	6143	0.6	51.7	90	0:180:180	0:90:270
B	12	6143	0.6	51.7	90	0:90:270	0:120:240
C	16	6143	0.6	51.7	90	0:180:180	0:45:315

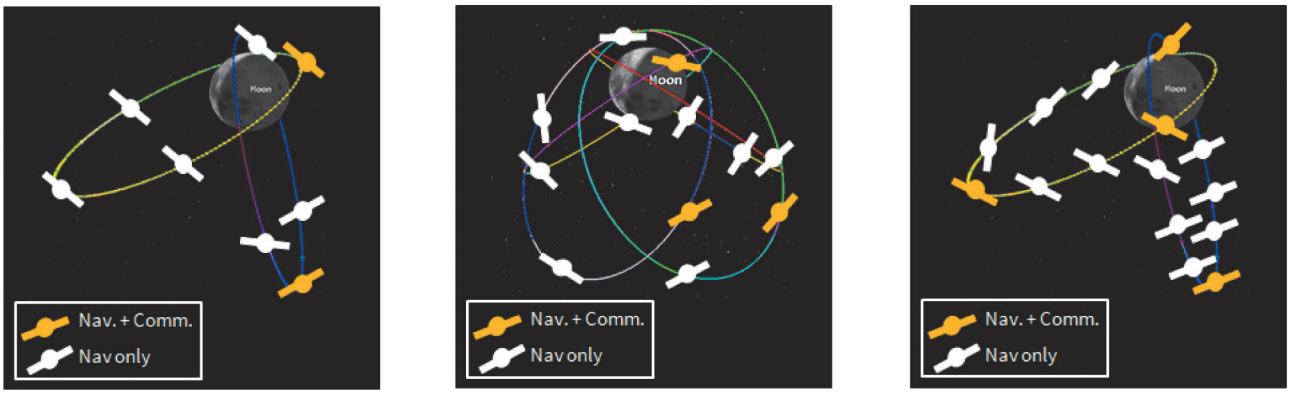

FIGURE 5 Three LNCSS case studies of a hybrid constellation type considered. All satellites provide navigation services and only 25% (highlighted in orange) provide both navigation and communication services (a) Case A: 6 navigation-only satellites and 2 navigation+communication-enabled satellites (b) Case B: 9 navigation-only satellites and 3 navigation+communication-enabled satellites (c) Case C: 12 navigation-only satellites and 4 navigation+communication-enabled satellites
The trade-off performance among case studies is analyzed in terms of design criteria and performance metrics for navigation and communication services, as well as SmallSat factors.

Kepler's third law in the lunar context, the orbital period of any LNCSS satellite in these case studies is $T_{orbital-period} = 12$ h (which considers $T_{orbital-period} = 2\pi\sqrt{\frac{a^3}{\mu_{moon}}}$ with Moon's standard gravitational parameter $\mu_{moon} = 4.9048695e^{12}$ m^3/s^2). The other two orbital parameters, namely, the initial mean anomaly and RAAN, are chosen to evenly distribute satellites within the LNCSS constellation.

3.1.2 | *Details of Case Studies*

As shown in Figure 5, three LNCSS constellation case studies, A, B, and C, are designed, with constellation sizes of 8, 12, and 16, respectively. Table 1 depicts the six orbital parameters associated with the satellites in each case study.

These case studies are evaluated against the criteria outlined in NASA's SRD (National Aeronautics and Space Administration, 2022), NASA's SCAWG (National Aeronautics and Space Administration, 2006), and a few other sources (Cozzens, 2021; European Space Agency, 2021; National Aeronautics and Space Administration, 2009; Rimani et al., 2021; Schier, 2022). This hybrid design is implemented by considering 25% of satellites within each constellation to provide communication services in addition to navigation services, i.e., $N_{comm} : N_{LNCSS} = 1:4$. This ratio was chosen because four visible LNCSS satellites at any lunar user are required to successfully compute a navigation solution, whereas only one visible communication-enabled satellite is required at any lunar user to perform data transfer to Earth. Note that an analysis on the effect of varying the number of communication satellites N_{comm} and the ratio $N_{comm} : N_{LNCSS}$ will be explored in future works.

3.2 | Modeling and Simulation Details

A high-fidelity simulation of the LNCSS case studies was conducted using the Systems Tool Kit (STK) software developed by Ansys (formerly under Analytical

Graphics, Inc.) (Ansys, 2022). An analysis was performed by considering the start time epoch to be 9 Nov 2025 00 : 00 : 00.000 UTC and the experiment time duration to be 15 days. This 15-day duration is equivalent to 30 full revolutions of any LNCSS satellite around the Moon, as one orbital period is 12 h (see Section 3.1.1)), thus allowing an analysis of the proposed design under various Earth-GPS-to-LNCSS geometries. In particular, the STK software was utilized to model the Earth-GPS constellation, LNCSS case studies, lunar users, and occultations caused by Earth and the Moon.

3.2.1 | *Modeling an LNCSS with Earth-GPS Time Transfer*

The simulated Earth-GPS constellation consists of 31 satellites with 8 satellites from Block IIR, 7 from IIRM, 12 from IIF, and 4 from Block III. At each LNCSS satellite, the received C/N_0 is simulated for all available Earth-GPS signals. For this step, various aspects were modeled, including the Earth-GPS antenna gain patterns (Donaldson et al., 2020), the attenuation due to free space path loss, the Earth-GPS receiver antenna (directional) onboard the LNCSS (Capuano et al., 2015), and its receiver front-end characteristics. Based on the received C/N_0 values, the pseudoranges and Doppler values were simulated and used to perform Earth-GPS time transfer. An Earth-GPS satellite is considered to be visible when the received C/N_0 value is greater than 15 dB-Hz for a continuous time duration of at least 40 s. A detailed explanation of the simulation setup and STK scenario is given in prior works (Bhamidipati et al., 2021, 2022b).

The timing filter is designed with the *time update* executed every $\Delta t = 60$ s and the *measurement update* executed using simulated pseudoranges and Doppler values when Earth-GPS signals are available (the maximum Earth-GPS continual outage period for an ELFO at 6143 km is approximately 3060 s). Please refer to prior works (Bhamidipati et al., 2021, 2022a, 2022b) for more details regarding successful convergence of the timing filter as the sampling interval Δt and the maximum Earth-GPS continual outage period (ECOP) are varied. The parameters of the process noise covariance matrix Q associated with the CSAC are defined as follows: $\mu_3 = 0$ and diffusion coefficients $\sigma_1 = 8.00 \cdot 10^{-11}, \sigma_2 = 2.72 \cdot 10^{-14}$, and $\sigma_3 = 0.0$. These diffusion coefficients are computed based on the equations derived in Section 2.1, for which the power spectral coefficients $h_0 = 1.28 \cdot 10^{-20}$ and $h_{-2} = 3.7411 \cdot 10^{-29}$ (taken from Krawinkel and Schön (2015)).

3.2.2 | *Modeling a Grid Array of Lunar Users*

Via STK (Ansys, 2022), the performance of the LNCSS constellation case studies was examined, as observed for users on the lunar surface. In particular, a grid array of users was examined, covering the lunar south pole (at lunar latitudes of 80° S and greater) with a resolution of 1° in both latitude and longitude grid points, resulting in a total of 334 grid points. At each grid point, key figures of merit were evaluated, as detailed in Sections 3.2.3) and 3.2.4), including navigation and communication service availability, coverage, tolerance to single-satellite failures, DOP, positioning and timing accuracy, and daily data volume. Furthermore, the navigation and communication service performance was examined with two different elevation masks: one at 5°, which is representative of a user with an unobstructed, open-sky view of the lunar sky, and one at 20°, which is representative of a user with restricted visibility, such as a user inside a lunar crater.

3.2.3 | Navigation Service Parameters and Lunar UERE Estimation

The simulation measurements generated independently in STK were passed to the timing filter in MATLAB. The timing filter ran for the entire experiment duration, over which the RMS estimation error in clock bias was evaluated, which represents the broadcast clock component of the lunar UERE formulation from Equation (6). Figure 6 shows the estimation errors associated with the three-state Kalman filter for an LNCSS satellite with an onboard CSAC. The RMS error (scaled by $c = 299792458$ m/s to express the errors in meters) in the Earth-GPS time transfer is demonstrated to be 2.37 m, while the maximum uncertainty is 4.67 m and the maximum error is approximately 8.76 m. Furthermore, because the RMS clock bias error exhibits a consistent trend across time for all satellites, the broadcast clock component is modeled as a constant value of $\sigma_{\text{clk, LNCSS}} = 2.37$ m for all satellites within the three LNCSS constellation case studies.

To characterize the lunar UERE at any LNCSS satellite, the same group delay and receiver noise error magnitudes are considered as with the Earth-GPS system, i.e., $\sigma_{\text{gd, LNCSS}} = 0.15$ m and $\sigma_{\text{rec, LNCSS}} = 0.1$ m. The broadcast ephemeris error component in the lunar UERE is modeled as $\sigma_{\text{eph, LCNSS}} = 3$ m, which is an order of magnitude higher than that of the legacy Earth GPS. Based on these values and the estimated broadcast clock component $\sigma_{\text{clk, LNCSS}}$, the lunar UERE is computed to be $\sigma_{\text{UERE, LCNSS}} = 3.86$ m.

The following navigation design criteria and performance metrics (as defined in Section 1.1) are modeled using several figures of merit available in the STK software, wherein all N_{LNCSS} LNCSS satellites are selected under assets in the coverage definition:

- Availability and failure tolerance: These performance criteria are evaluated using the coverage time figure of merit in STK, under the setting "Min Per Day" for the minimum percent availability of the system for each day over the simulation.
- GDOP: This performance criterion is evaluated using the DOP figure of merit in STK, and the 98th percentile GDOP is computed using the "Percent Below" setting for this STK figure of merit.

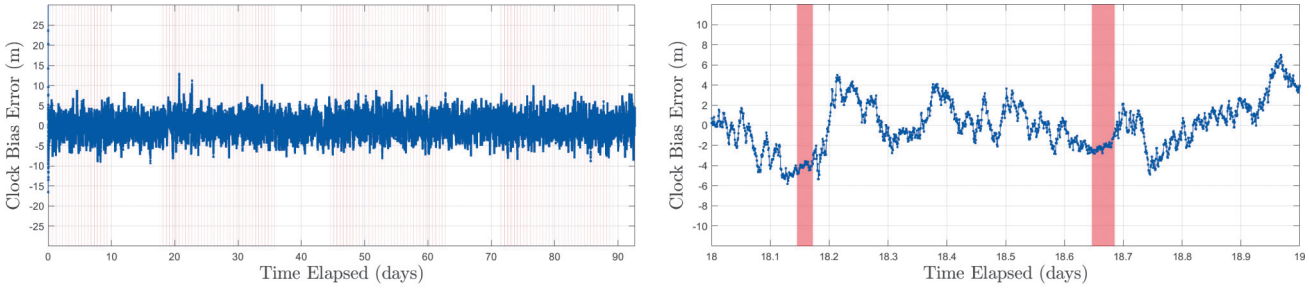

FIGURE 6 Timing estimation errors in the Earth-GPS time-transfer filter architecture for an LNCSS satellite in an ELFO with an onboard CSAC, where a) demonstrates the clock bias errors for the entire experiment duration and b) demonstrates the zoomed-in errors for a smaller time segment of 1 day

An RMS error of $\sigma_{\text{clk, LNCSS}} = 2.37$ m is demonstrated in the Earth-GPS time transfer, based on which the lunar UERE is computed as $\sigma_{UERE,LNCSS} = 3.86$ m. The red vertical bars indicate regions of ECOP (i.e., no Earth-GPS satellites are visible).

- Horizontal position, vertical position, and timing accuracy: These performance criteria are computed using the navigation accuracy related options under STK figures of merit, namely "HACC", "VACC", and "TACC", respectively, for which both the average and maximum accuracy 1σ error covariances are computed.

3.2.4 | Communication Service Parameters and Data Rate Estimation

To evaluate the attainable data rate for the LNCSS communication service, as outlined in Section 2.3, the parameters listed in Table 2 are assigned. Based on these values, the estimated data rate is computed to be $d_{Ka} = 44.7$ Mbps.

Similar to the navigation service performance evaluation, several STK figures of merit are utilized to model the following communication design criteria and performance metrics (as defined in Section 1.1):

- Availability and failure tolerance: These metrics are evaluated in a manner similar to the navigation service performance evaluation, using the coverage time STK figure of merit and evaluating the "Min Per Day" metric, but across the N_{comm} communication satellites that make up the communication service of the LNCSS. In STK, the N_{comm} satellites to consider are specified for this metric within the specified assets of the coverage definition.
- Time duration of availability t_{Ka} (defined in Section 2.3): To evaluate this metric, the coverage time STK figure of merit is first utilized to compute the "Min Percent Per Day" metric, wherein one communication satellite is selected for a particular time within the STK coverage definition list of assets. Then, the metric for each communication satellite is summed across all N_{comm} satellites to obtain the total system visibility.

3.2.5 | Parameters for SmallSat Factors

Based on Table 3, the total payload mass has an estimated power of $P_{payload-nav} = 83.9$ W. Utilizing data from past missions (Wertz et al., 2011), the mass of the navigation-only satellite is heuristically computed to be 133.5 kg. Furthermore, considering $D_{ant} = 1$ m (also the antenna diameter specified

TABLE 2
Communication System Parameters Used for Computing the Attainable Data Rate for Transfer Between the LNCSS Satellite and Earth

Parameter	Value
Transmission frequency f_{tx} (GHz)	27
Transmission power P_{tx} (W)	4.8
Receiver gain G_{rx} (dB)	55
Phase modulation index β (°)	60
Noise temperature T_{rx} (K)	29.2
Antenna efficiency	0.6
Antenna diameter (m)	1

in Table 2), Equation (13) is evaluated to compute the communication payload mass as 25.6 kg. With these results, the mass of a satellite providing both navigation and communication services is estimated to be 159.1 kg. Note that both of these satellite masses fall within the weight constraints acceptable for a SmallSat platform.

The total production costs are evaluated by setting a learning rate of $S = 85\%$ to match the parameter set by Hirshorn et al. (2017). Additionally, the space segment costs are computed by setting the inflation factor from 2010 to 2025 (the year for this simulation) as 1.35 (Wertz et al., 2011).

3.3 | Trade-off Analysis

A trade-off analysis is performed among the three LNCSS constellation case studies.

3.3.1 | *Navigation Design Performance Comparison*

The navigation design performance across all LNCSS case studies is compared for an elevation mask of 5°, with lunar UERE $\sigma_{\text{UERE, LCNSS}} = 3.86$ m (as estimated in Section 3.2.3)). Based on Table 4, all case studies demonstrate 100% availability and 100% coverage for navigation service over the lunar south pole region. Additionally, even during a single-satellite failure, both case B and case C satisfy

TABLE 3
Breakdown of Payload Equipment Onboard a Navigation-Only Satellite, with a CSAC as the Satellite Clock and the Corresponding Power Requirements (Parker et al., 2022; Pereira & Selva, 2020; Schmittberger & Scherer, 2020; Wertz et al., 2011)

Payload	Required Power (W)
Microchip CSAC (two units)	0.2
Earth-GPS receiver	14.7
Navigation signal generation unit	35
Frequency generation and upconversion unit	22
Remote terminal unit	12
Total payload power, $P_{payload-nav}$	83.9

TABLE 4
Navigation Service Performance Comparison for an Elevation Mask of 5°, with Lunar UERE $\sigma_{UERE,LNCSS} = 3.86$ m
The columns of mean performance denote the mean RMS error (RMSE) across the array of grid points, whereas the columns of max performance denote the RMSE of the worst-case grid point for each case study. See Section 3.2.3) for details on how the performance metrics and design criteria are computed.

LNCSS Case Study (# sats)	Performance metrics: At worst user grid point				Design criteria: Avg across user grid points					
	Availability (%)	Failure Tolerance (%)	Coverage (%)	GDOP	Horizontal Position RMSE (m)		Vertical Position RMSE (m)		Receiver Timing RMSE (μs)	
					Mean	Max	Mean	Max	Mean	Max
A (8)	100	97.9	100	8.95	5.62	61.62	15.00	277.22	0.03	0.62
B (12)	100	100	100	5.51	3.84	5.67	10.15	18.16	0.02	0.04
C (16)	100	100	100	4.38	3.15	4.72	7.63	15.32	0.01	0.03

TABLE 5

Navigation Service Performance Comparison for an Elevation Mask of 20°, with Lunar UERE $\sigma_{UERE,LNCSS} = 3.86$ m
The columns of mean performance denote the mean RMSE across the array of grid points, whereas the columns of max performance denote the RMSE of the worst-case grid point, for each case study. See Section 3.2.3) for details on how the performance metrics and design criteria are computed.

LNCSS Case Study (# sats)	Performance metrics: At worst user grid point averaged across time				Design criteria: Avg across user grid points					
	Availability (%)	Failure Tolerance (%)	Coverage (%)	GDOP	Horizontal Position RMSE (m)		Vertical Position RMSE (m)		Receiver Timing RMSE (μs)	
					Mean	Max	Mean	Max	Mean	Max
A (8)	77.51	54.11	53.29	246.24	14.75	4740.24	85.36	25620.85	0.19	56.94
B (12)	100	100	85.1	16.19	4.61	12.30	17.14	55.17	0.04	0.12
C (16)	100	100	100	7.24	4.12	7.04	14.06	29.88	0.03	0.07

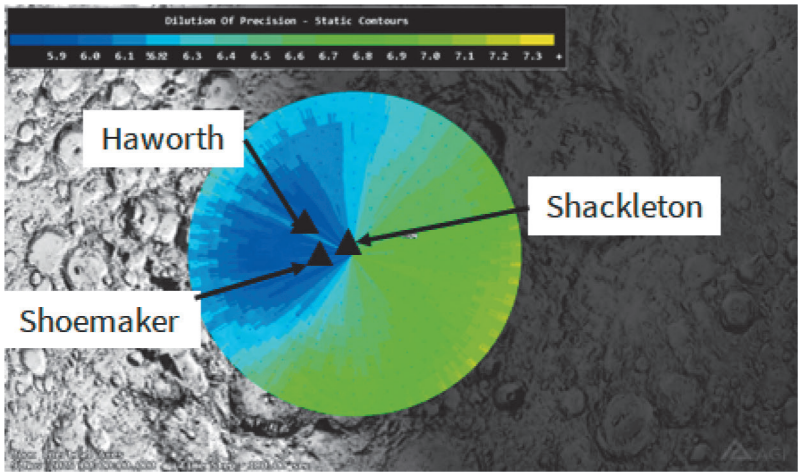

FIGURE 7 GDOP variation in the lunar south pole region for case C, with an elevation mask of 20°
For intuition, a few prominent craters in the lunar south pole region are also marked, namely, the Shoemaker, Shackleton, and Haworth craters. As expressed in Table 5, the worst-case grid point has an average GDOP of 7.24 for 20°.

NASA's requirement (National Aeronautics and Space Administration, 2022) of having at least 98% navigation service availability. Case C also satisfies NASA's recommended horizontal position accuracy with 3σ less than 10 m (i.e., $1\sigma < 3.33$ m) (National Aeronautics and Space Administration, 2022) and the global exploration community's prescribed 3D position accuracy of less than 50 m (Cozzens, 2021). Furthermore, all cases studies satisfy the receiver clock timing requirements, with an accuracy within the prescribed threshold of 1 μs. Table 5 of Isik et al. (2020) provides an interpretation of the GDOP values, according to which <1 is ideal, 1–2 is excellent, 2–5 is good, 5–10 is moderate, 10–20 is fair, and <20 is poor. Based on this interpretation, case A and case B fall under the moderate category whereas case C falls under the good category.

The position and timing accuracies are additionally analyzed for an elevation mask of 20° in Table 5 with lunar UERE $\sigma_{\text{UERE, LCNSS}} = 3.86$ m (same as that for the 5° elevation mask). Even for a higher elevation mask of 20°, case C still satisfies the global exploration community's desired 3D position accuracy of less than 50 m.

In Figure 7, the GDOP variation for case C across the lunar south pole region is illustrated for an elevation mask of 20°. These GDOP values, varying

TABLE 6
Communication Design Performance Comparison for an Elevation Mask of 5° and a Data Rate of $d_{\text{Ka}} = 44.7$ Mbps See Section 3.2.4) for details on how the performance metrics and design criteria are computed.

LNCSS Case Study (# comm. sats, # total sats)	Performance metrics: At worst user grid point			Design criteria: Avg across grid points	Daily Data Volume (GB)
	Availability (%)	Failure Tolerance (%)	Coverage (%)	Summed Daily Availability t_{Ka} of LNCSS–Earth Data Link (s) (minimum among 15 days)	
A (2, 8)	100	43.75	100	160320	895.79
B (3, 12)	100	80.15	100	246720	1791.24
C (4, 16)	100	100	100	336012	1378.55

between 5.9 and 7.3 (falling under the moderate category based on Isik et al. (2020)), are indicative of restricted satellite visibility caused by the lunar terrain, as experienced by a user within a lunar crater or canyon, for example. As a result, slightly degraded position and timing accuracy is observed, as compared with the scenario with an elevation mask of 5°, representing a user with an unobstructed view of the lunar sky.

3.3.2 | *Communication Design Performance Comparison*

Next, the communication design performance is compared across all LNCSS case studies for an elevation mask of 5° and a data rate of $d_{\text{Ka}} = 44.7$ Mbps (as estimated in Section 3.2.4)). Based on Table 6, cases A and B, which have fewer satellites, are observed to be less tolerant to single-satellite failures, with failure tolerance availabilities of 43.75% and 80.15%, respectively, while case C maintains 100% failure tolerance availability. Nevertheless, both cases B and C are observed to satisfy the high data rate requirement of 75% communication availability, even under single-satellite failures (National Aeronautics and Space Administration, 2022). Under the design criteria, a derived metric based on the summed daily availability t_{Ka} of the LNCSS–Earth data link is compared, wherein summation is performed across the daily availability of each communication-enabled satellite within the LNCSS constellation. As described in Section 2.3, t_{Ka} is computed on a per day basis. To compute this derived metric for each case study, the minimum t_{Ka} is computed among all 15 days at each grid point; then, the derived metric is reported to be the average across all grid points. As expected, the value of this derived metric/design criterion is proportional to N_{comm}. Additionally, this derived metric/design criterion is independent of the elevation mask considered and thus has the same values in Table 6 and Table 7. The daily data volume between a lunar user and Earth across all case studies satisfies the desired values specified by multiple prior works, i.e., greater than 160 GB based on Rimani et al. (2021), between 240 and 2400 GB as per European Space Agency (2021), and $>$ 600 GB based on Schier (2022).

In Table 7, a communication performance comparison is presented for 20° with a data rate of 44.7 Mbps (same as that considered for the 5° elevation mask). While case A falls to 86.50% for 20°, compared with 100% for 5°, all case studies satisfy the requirement of at least 75% communication availability. A communication coverage

TABLE 7
Communication Design Performance Comparison for an Elevation Mask of 20° and a Data Rate of $d_{Ka} = 44.7$ Mbps See Section 3.2.4) for details on how the performance metrics and design criteria are computed.

LNCSS Case Study (# comm. sats, # total sats)	Performance metrics: At worst user grid point			Design criteria: Avg across grid points	Daily Data Volume (GB)
	Availability (%)	Failure Tolerance (%)	Coverage (%)	Summed Daily Availability t_{Ka} of LNCSS–Earth Data Link (s) (minimum among 15 days)	
A (2,8)	86.50	15.57	100	160320	895.79
B (3, 12)	100	51.22	100	246720	1791.24
C (4, 16)	100	88.32	100	336012	1378.55

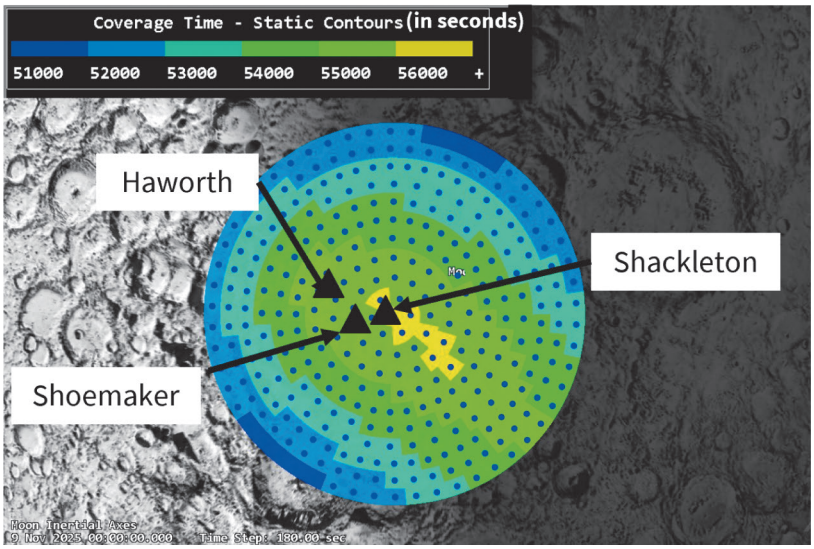

FIGURE 8 Variation in the minimum availability per day t_S of one LNCSS communication satellite across the lunar south pole region (greater than 80° S latitudes) for case C, with an elevation mask of 20°
For intuition, a few prominent craters are also marked, namely, the Shoemaker, Shackleton, and Haworth craters.

of 100% is also demonstrated across all case studies. Additionally, the daily data volume exceeds 895.79 GB, which satisfies the desired preliminary requirements taken from different sources (European Space Agency, 2021; Rimani et al., 2021; Schier, 2022). Even under restricted satellite visibility, all case studies exhibit daily data volumes of greater than 461 GB, where 461 GB is the daily volume of data being transmitted by the LRO (National Aeronautics and Space Administration, 2009). Note that the daily data volumes for elevation masks of 5° and 20° are the same because D_{Ka} is considered the bottleneck for communication data transfer (as discussed in Section 2.3).

In Figure 8, the minimum availability of one LNCSS communication satellite per day is plotted across all grid points for case C with an elevation mask of 20°. These values are observed to be around 15 h (≈ 54000 s). As explained in Section 2, the bottleneck for communication data transfer between a lunar user and Earth is

TABLE 8
Comparison of Space Segment Costs Across the LNCSS Case Studies
The heuristic relationships used to calculate the total development and production costs in Brown (2002), Pereira and Selva (2020), and Wertz et al. (2011) are relevant for 2010 costs; thus, an inflation factor from 2010 to 2025 of 1.35 is considered (Wertz et al., 2011).

LNCSS Case Study (# comm. sats, # total sats)	Total Dev. Cost [FY2025$M]		Total Prod. Cost [FY2025$M]		Total Space Segment Cost of LNCSS [FY2025$M]	Average LNCSS Satellite Cost [FY2025$M]
	Comm. Payload	Nav.-Only Satellite	Comm. Payload	Nav.-Only Satellite		
A (2, 8)	39.52	19.92	11.15	64.03	134.62	16.83
B (3, 12)	39.52	19.92	15.21	87.33	161.98	13.50
C (4, 16)	39.52	19.92	18.96	108.85	187.25	11.70

the Ka-band segment, which accommodates communication between the LNCSS satellite and Earth. Given an available data rate of d_S between the lunar user and the LNCSS satellite, one can determine the number of lunar users that can communicate with Earth on a daily basis by equating the data transferred across both segments, i.e., $d_{Ka}t_{Ka} = d_S t_S$. For example, considering $d_S = 36$ kbps from National Aeronautics and Space Administration (2022), the number of lunar users that can continuously communicate with Earth in case A is 44.7 Mbps $\times$ 160320/(36 $\times$ 54000) = 3686.

3.3.3 | *Comparison of Space Segment Costs*

Table 8 shows a breakdown of the total development cost and total production cost of the communication payload and navigation-only satellite, as well as the total space segment cost for all case studies. As mentioned in Section 2.4, an evaluation of other components of the overall cost (except the total space segment cost) will be explored in future works. Furthermore, the average satellite cost across all case studies is computed to be less than 17 [FY2025$M], which is comparable to NASA's low-cost CAPSTONE mission that was recently launched in June 2022 (Cheetham, 2021) with a cost of approximately 20 [FY2022$M].

Additional launch cost considerations can also be estimated in comparison to NASA's LRO and Lunar Crater Observation and Sensing Satellite (LCROSS), which were launched in June 2009 (National Aeronautics and Space Administration, 2009). The combined payload mass of both the LRO and LCROSS at the time of launch accounted for 2807 kg, and the total cost for launch services to the Moon was 136.2 [FY2009$M] (Diller, 2006). For case C, the largest proposed constellation design at 16 total satellites, the estimated combined mass is 2239 kg. Adjusting for inflation metrics from 2009 to 2025 with a value of 1.38 (taken from Wertz et al. (2011)), the total launch costs for the largest LNCSS design proposed in this study are assumed to be less than 188.2 [FY2025$M], resulting in a maximum estimation of 375.5 [FY2025$M] for the total production, development, and launch costs of these LNCSS case studies. In Section 3.2.5), the inflation factor from 2010 to 2025 was 1.35; however, because the LCROSS mission was launched in 2009, a value that accounts for inflation from 2009 to 2025 was considered, i.e., 1.38. Note that this scenario differs from the remainder of the experimental analysis, in which the heuristic relationships were considered with respect to 2010 and a different inflation factor of 1.35 was considered.

4 | CONCLUSION

In summary, design and performance considerations for a SmallSat-based LNCSS were analyzed to provide reliable navigation and communication services at the lunar south pole. Through high-fidelity STK simulations, three case studies for an ELFO and a CSAC were examined, via an Earth-GPS time-transfer architecture. In particular, the case studies were examined in terms of navigation and communication service availability, coverage, tolerance to single-satellite failure, lunar UERE, DOP, positioning and timing accuracy, daily data volume, space segment costs, and onboard SWaP. A trade-off analysis in satisfying the preliminary design criteria outlined by various stakeholders such as NASA, the ESA, and the global exploration community was also performed. For elevation masks of 5° (open-sky) or 20° (crater), we demonstrate that case C, which has a larger constellation size of 16, performs most consistently across all design criteria and performance metrics. Notably, in contrast to the other case studies, case C maintains a failure tolerance of 100% under single-satellite failure in terms of navigation and 88.32% in terms of communication, while incurring the lowest average per satellite cost of 11.7 [FY2025$M].

ACKNOWLEDGMENTS

We thank the Analytical Graphics, Inc. Educational Alliance Program for providing us with the STK software license to perform this research work. We also thank Keidai Ilyama and Chris Flood for insightful discussions related to this work as well as Asta Wu for reviewing this paper.

REFERENCES

Ansys. (2022). Systems Tool Kit (STK) [Accessed Mar 16, 2023]. https://www.ansys.com/products/missions/ansys-stk

Balossino, A., & Davarian, F. (2022). The plan to give the Moon decent wireless coverage [Accessed Mar 16, 2023]. *IEEE Spectrum*. https://spectrum.ieee.org/lunar-communications

Bhamidipati, S., Mina, T., & Gao, G. (2021). Design considerations of a lunar navigation satellite system with time-transfer from Earth-GPS. *Proc. of the 34th International Technical Meeting of the Satellite Division of the Institute of Navigation (ION GNSS+ 2021)*, St. Louis, MO. 950–965. https://doi.org/10.33012/2021.18021

Bhamidipati, S., Mina, T., & Gao, G. (2022a). Time transfer from GPS for designing a SmallSat-based lunar navigation satellite system. *NAVIGATION, 69*(3). https://doi.org/10.33012/navi.535

Bhamidipati, S., Mina, T., & Gao, G. (2022b). A case study analysis for designing a lunar navigation satellite system with time-transfer from earth-GPS. *Proc. of the 35th International Technical Meeting of the Institute of Navigation,* Long Beach, CA. 407–419. https://doi.org/10.33012/2022.18202

Bhamidipati, S., Mina, T., Sanchez, A., & Gao, G. (2022). A lunar navigation and communication satellite system with Earth-GPS time transfer: Design and performance considerations. *Proc. of the International Technical Meeting of the Satellite Division of the Institute of Navigation (ION GNSS+ 2022),* Denver, CO. 537–553. https://doi.org/10.33012/2022.18365

Brown, C. D. (2002). *Elements of spacecraft design*. American Institute of Aeronautics; Astronautics, Inc. 447–502. https://doi.org/10.2514/5.9781600861796.0447.0502

Capuano, V., Basile, F., Botteron, C., & Farine, P. A. (2015). GNSS-based orbital filter for Earth Moon transfer orbits. *Journal of Navigation*, *69*(4), 745–764. https://doi.org/10.1017/s0373463315000843

Cheetham, B. (2021). Cislunar autonomous positioning system technology operations and navigation experiment (CAPSTONE). https://doi.org/10.2514/6.2021-4128.vid

Cohen, B., Lawrence, S., Denevi, B., Glotch, T., Hurley, D., Neal, C., Robinson, M., Watkins, R., & Weber, R. (2020). Lunar missions for the decade 2023–2033 [Accessed Mar 16, 2023]. *A White Paper submitted to the 2023 Planetary Science Decadal Survey*. https://www.lpi.usra.edu/leag/reports/LEAG-Mission-Priorities-v4.pdf

Cozzens, T. (2021). Galileo will help lunar pathfinder navigate around Moon [Accessed Mar 16, 2023]. *GPS World*. https://www.gpsworld.com/galileo-will-help-lunar-pathfinder-navigate-around-moon

Diller, G. (2006). NASA awards launch services for lunar mission [Accessed Mar 16, 2023]. *NASA Newsworld*. https://www.nasa.gov/home/hqnews/2006/jul/HQ_C06042_LRO_contract.html

Donaldson, J. E., Parker, J. J., Moreau, M. C., Highsmith, D. E., & Martzen, P. D. (2020). Characterization of on-orbit GPS transmit antenna patterns for space users. *NAVIGATION*, *67*(2), 411–438. https://doi.org/10.1002/navi.361

Ely, T. A. (2005). Stable constellations of frozen elliptical inclined lunar orbits. *The Journal of the Astronautical Sciences*, *53*(3), 301–316. https://doi.org/10.1007/bf03546355

Ely, T. A., & Lieb, E. (2006). Constellations of elliptical inclined lunar orbits providing polar and global coverage. *The Journal of the Astronautical Sciences*, *54*(1), 53–67. https://doi.org/10.1007/bf03256476

Esper, J. (2022). *Draft lunanet interoperability specification* (tech. rep.) [Accessed Mar 16, 2023]. National Aeronautics and Space Administration. https://ntrs.nasa.gov/citations/20220010998

European Space Agency. (2021). Moonlight initiative: Lunar communications and navigation services (lcns) [Accessed Mar 16, 2023]. *Call for Ideas and Use Cases*. https://commercialisation.esa.int/opportunities/moonlight-initiative-lunar-communications-and-navigation-services-lcns-call-for-ideas-and-use-cases/

European Space Agency. (2023). Remote terminal units [Accessed Mar 24, 2023]. https://www.esa.int/Enabling_Support/Space_Engineering_Technology/Onboard_Computers_and_Data_Handling/Remote_Terminal_Units

Flahaut, J., Carpenter, J., Williams, J.-P., Anand, M., Crawford, I., van Westrenen, W., Füri, E., Xiao, L., & Zhao, S. (2020). Regions of interest (ROI) for future exploration missions to the lunar south pole. *Planetary and Space Science*, *180*. https://doi.org/10.1016/j.pss.2019.104750

Folta, D., & Quinn, D. (2006). Lunar frozen orbits. *Proc. of the AIAA/AAS Astrodynamics Specialist Conference and Exhibit*, Keystone, CO, 6749. https://doi.org/10.2514/6.2006-6749

Hamera, K., Mosher, T., Gefreh, M., Paul, R., Slavkin, L., & Trojan, J. (2008). An evolvable lunar communication and navigation constellation concept. *Proc. of the 2008 IEEE Aerospace Conference*, Big Sky, MT. 1–20. https://doi.org/10.1109/aero.2008.4526326

Hirshorn, S. R., Voss, L. D., & Bromley, L. K. (2017). *NASA systems engineering handbook* (tech. rep.).

Iannone, C., Carosi, M., Eleuteri, M., Stallo, C., Lauro, C. D., & Musacchio, D. (2021). Four satellites to navigate the moon's south pole: An orbital study. *Proc. of the 34th International Technical Meeting of the Satellite Division of The Institute of Navigation (ION GNSS+ 2021),* St. Louis, MO. 981–1003. https://doi.org/10.33012/2021.18022

Isik, O. K., Hong, J., Petrunin, I., & Tsourdos, A. (2020). Integrity analysis for GPS-based navigation of UAVs in urban environment. *Robotics*, *9*(3), 66. https://doi.org/10.3390/robotics9030066

Israel, D. J., Mauldin, K. D., Roberts, C. J., Mitchell, J. W., Pulkkinen, A. A., Cooper, L. V. D., Johnson, M. A., Christe, S. D., & Gramling, C. J. (2020). LunaNet: A flexible and extensible lunar exploration communications and navigation infrastructure. *Proc. of the 2020 IEEE Aerospace Conference*, Big Sky, MT. 1–14. https://doi.org/10.1109/aero47225.2020.9172509

Krawinkel, T., & Schön, S. (2015). Benefits of receiver clock modeling in code-based GNSS navigation. *GPS Solutions*, *20*(4), 687–701. https://doi.org/10.1007/s10291-015-0480-2

McManus, L., & Schaub, H. (2016). Establishing a formation of small satellites in a lunar flower constellation. *The Journal of the Astronautical Sciences*, *63*(4), 263–286. https://doi.org/10.1007/s40295-016-0096-y

Mortari, D., Wilkins, M. P., & Bruccoleri, C. (2004). The flower constellations. *The Journal of the Astronautical Sciences*, *52*(1–2), 107–127. https://doi.org/10.1007/bf03546424

Murata, M., Kawano, I., & Kogure, S. (2022). Lunar navigation satellite system and positioning accuracy evaluation. *Proc. of the 2022 International Technical Meeting of the Institute of Navigation,* Long Beach, CA. 582–586. https://doi.org/10.33012/2022.18220

Nallapu, R. T., Vance, L. D., Xu, Y., & Thangavelatham, J. (2020). Automated design architecture for lunar constellations. *Proc. of the 2020 IEEE Aerospace Conference*, Big Sky, MT. 1–11. https://doi.org/10.1109/aero47225.2020.9172381

National Aeronautics and Space Administration. (2006). Space communication architecture working group [Accessed Mar 16, 2023]. *NASA Space Communication and Navigation Architecture Recommendations for 2005–2030. Final Report*. https://syzygyengineering.com/2007/SCAWG_Report.pdf

National Aeronautics and Space Administration. (2009). Lunar reconnaissance orbiter (LRO): Leading NASA's way back to the moon; Lunar crater observation and sensing satellite (LCROSS): NASA's mission to search for water on the Moon. *Press Kit*. https://www.nasa.gov/pdf/360020main_LRO_LCROSS_presskit2.pdf

National Aeronautics and Space Administration. (2022). Lunar communications relay and navigation systems (LCRNS). *Preliminary Lunar Relay Services Requirements Document (SRD)*. https://esc.gsfc.nasa.gov/projects/LCRNS

Parker, J. J., Dovis, F., Anderson, B., Ansalone, L., Ashman, B., Bauer, F. H., D'Amore, G., Facchinetti, C., Fantinato, S., Impresario, G., McKim, S. A., Miotti, E., Miller, J. J., Musmeci, M., Pozzobon, O., Schlenker, L., Tuozzi, A., & Valencia, L. (2022). The lunar GNSS receiver

experiment (LuGRE). *Proc. of the 2022 International Technical Meeting of the Institute of Navigation,* Long Beach, CA. 420–437. https://doi.org/10.33012/2022.18199

Pereira, F., & Selva, D. (2020). Exploring the design space of lunar GNSS in frozen orbit conditions. *Proc. of the IEEE/ION Position, Location and Navigation Symposium (PLANS 2020),* Portland, OR. 444–451. https://doi.org/10.1109/plans46316.2020.9110202

Pereira, F., & Selva, D. (2022). Analysis of navigation performance with lunar GNSS evolution. *Proc. of the 2022 International Technical Meeting of the Institute of Navigation,* Long Beach, CA. 514–529. https://doi.org/10.33012/2022.18210

Proakis, J. G., & Salehi, M. (2008). *Digital communications*. McGraw-Hill Higher Education.

Rimani, J., Mascolo, L., & Fraire, J. A. (2021). A parametric data handling evaluation framework for autonomous lunar networks. *CEAS Space Journal*, *14*(2), 365–376. https://doi.org/10.1007/s12567-021-00390-4

Schier, J. (2022). Lunanet overview [Accessed Mar 16, 2023]. *NESCUnique Science from the Moon in the Artemis EraWorkshop*. https://www.nasa.gov/sites/default/files/atoms/files/lunanet_overview_to_nesc_lunar_science_workshop_2022-6-7.pdf

Schmittberger, B. L., & Scherer, D. R. (2020). A review of contemporary atomic frequency standards. *arXiv preprint arXiv:2004.09987*. https://arxiv.org/pdf/2004.09987.pdf

Stutzman,W. L., & Thiele, G. A. (2013). *Antenna theory and design (3rd ed.)*. John Wiley & Sons. https://doi.org/10.1109/9780470544174.part1

Tai,W., Cosby, M.,& Lanucara, M. (2020). Lunar communications architecture study report (v1.2) [Accessed on Mar 16, 2023]. *Interagency Operations Advisory Group, Lunar Communications Architecture Working Group*. https://ntrs.nasa.gov/citations/20210006495

Thompson, J., Haygood, H., & Kezirian, M. (2010). Design and analysis of lunar communication and navigation satellite constellation architectures. *Proc. of the AIAA SPACE 2010 Conference & Exposition*, Anaheim, CA. https://doi.org/10.2514/6.2010-8644

Van Dierendonck, A. J., & McGraw, J. (1984). Relationship between Allan variances and Kalman filter parameters. *Proc. of the 16th Annual Precise Time and Time Interval Systems and Applications Meeting*, 273–293. https://www.ion.org/publications/abstract.cfm?articleID=16168

Wertz, J. R., Everett, D. F., & Puschell, J. J. (2011). *Space mission engineering: The new SMAD*. Microcosm Press. [Accessed on Aug 7, 2023] http://www.sme-smad.com

Whitley, R., & Martinez, R. (2016). Options for staging orbits in cislunar space. *Proc. of the 2016 IEEE Aerospace Conference*, Big Sky, MT. 1–9. https://doi.org/10.1109/aero.2016.7500635

Winternitz, L. B., Bamford, W. A., Long, A. C., & Hassouneh, M. (2019). GPS based autonomous navigation study for the lunar Gateway. *Proc. of the Annual American Astronautical Society (AAS) Guidance, Navigation, and Control Conference*, (AAS 19-096), Breckenridge, CO.

Zucca, C., & Tavella, P. (2005). The clock model and its relationship with the allan and related variances. *IEEE Transactions on Ultrasonics, Ferroelectrics and Frequency Control*, *52*(2), 289–296. https://doi.org/10.1109/tuffc.2005.1406554

How to cite this article: Bhamidipati, S., Mina, T., Sanchez, A., & Gao, G. (2023). Satellite constellation design for a lunar navigation and communication system. *NAVIGATION, 70*(4). https://doi.org/10.33012/navi.613